Enhanced structural and magnetic properties of fcc colloidal crystals of cobalt nanoparticles

S. Costanzo, A. Ngo, V. Russier, P. Albouy, G. Simon, Ph. Colomban, C. Salzemann, J. Richardi, I. Lisiecki

Enhanced structural and magnetic properties of fcc colloidal crystals of cobalt nanoparticles

Nanoscale 12, 24020 (2020) DOI: 10.1039/d0nr05517d

S. Costanzo,[a] A. T Ngo,[a] V. Russier,[b] P. A. Albouy,[c] G. Simon,[a] Ph. Colomban,[a] C. Salzemann,[a] J. Richardi[d] and I. Lisiecki*[a]

[a]Sorbonne Université, CNRS, De la Molécule aux Nano-Objets: Réactivité, Interactions Spectroscopies, MONARIS, 75005, Paris France
[b]ICMPE UMR 7182 CNRS and Université UPE, 2-8 rue Henri Dunant, 94320 Thiais, France.

[c]Laboratoire de Physique des Solides, Université Paris-Sud, 91405 Orsay, France

[d]Sorbonne Université, CNRS, Laboratoire de Chimie Théorique, LCT, F. 75005 Paris, France

Keywords: fcc-Co, nanocrystals, fcc colloidal crystals, anisotropy, magnetic dipolar interaction, crystal nucleation, solubility parameters, Flory theory of solvation

* Address correspondence to isabelle.lisiecki@upmc.fr

Abstract

We report the elaboration of supercrystals made of dodecanoic acid-coated 8.1 nm-Co nanocrystals with controlled supercrystallinity, morphology and magnetic properties. The supercrystal growth is controlled using the solvent-mediated ligand-ligand interaction strategy. Either face-centered cubic supercrystalline films or single colloidal crystals composed of cobalt nanocrystals are obtained. The change of supercrystal morphology is explained by a Flory-type solvation theory using Hansen solubility colloidal parameters. The use of the same batch of Co nanocrystals for the fabrication of the supercrystalline films and colloidal crystals enables an accurate comparative structural and magnetic studies using (high-resolution) transmission electron microscopy, field emission gun scanning electron microscope, grazing incidence small-angle X-ray scattering and vibrating sample magnetometer. The nearest neighbor distance between nanoparticles is interpreted using theoretical models proposed in the literature. We evidence the increase in both the geometric anisotropy and the magnetic dipolar interactions for the colloidal crystals compared to the supercrystalline films.

1. Introduction

3D self-assembly of inorganic nanocrystals (NCs) into micrometer-scale ordered arrays (also called supercrystals) constitutes attractive advanced materials.[1–3] Resulting from collective interactions between neighboring NCs, they exhibit new mechanical,[4] transport,[5] optical, vibrational,[6] chemical (stability against oxidation and coalescence) and magnetic properties.[7] When the building units are magnetic, magnetic properties of these assemblies are greatly influenced by the dipolar interactions (DDI) between NCs. At sufficiently high concentrations, the interparticle dipolar interactions can produce “collective states” below a system dependent transition temperature Tc. The observed collective states are almost invariably “disordered” and thus called “superspin glasses” (SSG) as they show many of the phenomenology found in atomic spin glasses. [8,9] In a previous study, we have shown that fcc supercrystalline films made of cobalt NPs, are characterized by SSG properties. [10] Further increasing inter-particle correlations, the SSG state is predicted to transform into long-range ordered dipolar superferromagnetic (SFM) state. The collective ferromagnetic ordering induced by the dipolar interactions (DDI) is expected to present a great interest for technological applications. [11,12] However, a clear-cut experimental evidence of a dipolar SFM state in real 3D NP assemblies has not yet been reported. To the best of our knowledge the only case of SFM is obtained in cases where additional super-exchange interations play an important role.[13] Such a dipolar SFM state results necessarily from strong DDI and given the known properties of dipolar systems, it is expected to occur in assemblies of NCs provided they meet the following conditions: the NCs must be organized on either a well ordered supercrystal of face-centered cubic (fcc), hexagonal close packed (hcp), body centered tetragonal (bct) symmetry or a close packed structure (random close packed, RCP) on the one hand and characterized by either a very weak anisotropy or a strongly textured distribution of easy axes on the other hand.[8, 14-16] Single supercrystals (also called colloidal crystals) made of densely and regularly packed NCs constitute potential candidates for this aim.[8] Today, few examples of colloidal crystals have been

reported in the literature. The magnetic ones are minority,[4,17–23] and their magnetic properties have never been studied. In recent years several theories were developed to describe the interaction and geometry of nanoparticle assemblies.[24,25]

In this paper, we investigate both experimentally and theoretically the formation and properties of colloidal crystals of dodecanoic acid-coated 8.1 nm-Co NCs. In order to obtain this morphology, the NC solution in hexane is co-evaporated in the presence of ethanol.[26] Through a comprehensive structural investigation involving (high-resolution) transmission electron microscopy ((HR)TEM), grazing incidence small-angle X-ray scattering (GISAXS) and field emission gun scanning electron microscope (FEG-SEM), we evidence for the first time the formation of highly ordered fcc colloidal crystals of Co NCs, with regular shapes, the density packing of which is higher compared to the supercrystalline films composed of the same Co NCs. In order to explain the formation of single supercrystals with well- characterized shape, the interaction between the NCs is estimated with the help of a Flory-type theory using Hansen solubility parameter.[27-29] This enables us to predict the amount of ethanol in hexane necessary to induce attraction between the particles, which leads to the nucleation and growth of single supercrystals. The use of the same batch of Co NCs, to form the different types of supercrystals, allows us to accurately compare the structural properties of supercrystalline films and colloidal crystals. Based on this accurate structural study, specific magnetic properties of colloidal crystals are evidenced.

2. Experimental section

2.1. Chemical

All materials were used as purchased without further purification. Cobalt acetate and ethanol (VWR), isooctane and hexane (Sigma Aldrich), sodium di(ethylhexyl) sulfosuccinate (Na(AOT)) (Fluka), and sodium borohydride and dodecanoic acid (Acros). The synthesis of cobalt(II) bis(2-ethylhexyl)sulfosuccinate, $Co(AOT)_2$, has been described previously.[30]

2.2. Synthesis of Dodecanoic Acid Coated 8.1 nm-Co NCs

Cobalt NCs coated by dodecanoic acid chains are synthesized by chemical reduction in reverse micelles as described in a previous paper.[31] The size polydispersity is reduced by controlling the reducing agent (sodium borohydride) concentration. The NCs are dispersed in hexane. The mean diameter and size dispersion of the particles (determined with more than 500 particles) are equal to 8.1 nm and 11%, respectively. A second batch of NCs, referred to in the following as batch 2, following the same protocol and leading to almost similar NCs (8.5 nm and 10 %), is synthesized, in order to serve as a reference for the magnetic measurements in the dispersed solution.

2.3. Synthesis of 3D fcc Supercrystalline Film made of 8.1 nm-Co NCs

The 3D supercrystalline film is prepared by horizontally immersing a HOPG graphite substrate (10 x 5 mm^2) into a colloidal solution of Co NCs in hexane, which the overall concentration is 8 10^{-3} M. Solvent evaporation takes place at 35 °C under nitrogen and lasts approximately 24 h.[32,33]

2.4. Synthesis of Colloidal Crystals made of 8.1 nm-Co NCs

A first population of colloidal crystals made of 8.1 nm-Co NCs is produced by diffusion of ethanol vapor into a NCs colloidal solution: One beaker (*beaker 1*) is filled with 200 μL of a NC ($6\ 10^{-3}$ M of atomic cobalt) colloidal solution in hexane, at the bottom of which a silicon wafer is positioned horizontally. Another beaker (*beaker 2*), having the same size, is filled with 100 μL of ethanol. The beakers 1 and 2 are positioned into a third one, which is sealed and left at room temperature. Total evaporation of the solvent in beaker 1 occurs within approximately 20 h. A second population of colloidal crystals made with the same batch of Co NCs, is produced by using the same process except for the volume of ethanol in the beaker 2 which is 800 μL (instead of 100 μL). In this latter case, total evaporation of the solvent in beaker 1 occurs within approximately 8h. The as-prepared samples are then investigated by SEM, SEM-FEG and GISAXS techniques.

2.5. Apparatus

Transmission Electron Microscopy (TEM) study is performed using a JEOL JEM-1011 microscope at 100 kV.

Scanning Electron Microscopy (SEM) studies are performed using a scanning electron microscope (SEM, JEOL 5510 LV) and a field emission gun scanning electron microscope (FEG-SEM, Hitachi Su-70).

Grazing Incidence Small-angle X-ray scattering (GISAXS) measurements are carried out using a rotating anode generator operated with a small-size focus (copper anode; focus size 0.2 mm x 0.2 mm; 50kV, 30mA). Beam collimation and monochromatization is ensured by a parallel beam multilayer graded mirror optic. The sample is mounted on rotating and translation stages and the diffraction patterns are recorded on photo-stimulable imaging plates. Vacuum pipes are inserted between the sample and the imaging plate to reduce air scattering. During GISAXS measurement the incident beam probes a section ca. 0.8mm in width and extending the sample along.

Magnetic measurements are carried out on a vibrating sample magnetometer (VSM) from Quantum design with a field of 2 mT for the zero-field cooled (ZFC)/field cooled (FC) susceptibility curves, and with fields up to 5 T for the magnetization curves. All magnetic measurements are carried out with the applied field parallel to the substrate. In the ZFC measurement, the sample is cooled down from 300 K to 3 K with no field and then heated to 300 k in a small field of 2 mT while the magnetization $M_{ZFC}(T)$ of the sample is recorded. Then for the FC measurement, the sample is cooled again to 3 K under the same applied field and the magnetization $M_{FC}(T)$ is recorded. Hysteresis curves are taken at 3 K for all the samples.

2.6. Theory: interaction model

Due to the slow evaporation of the solvent (time scale of hours), the nanoparticles can adapt to the new situations by diffusion (time scale of 0.1 ms) and the rapid motion of the ligand chain (about 300 faster than the particle motion). Therefore, a thermodynamic theory can be applied to estimate the interaction and distance between the nanoparticles. To compute the interaction between the NCs, we use a modified Flory theory which has been explained elsewhere.[27,28] The calculations are carried out with the help of the code NanoForceG, a home-written program. The interaction energy between the NCs is made of four terms: the Van-der-Waals attraction between the metallic cores of the NCs, the free energy of mixing of the ligands, the elastic compression of the ligands, and the magnetic interaction

between the cores. The free energy of mixing is based on the interaction parameter χ_{12} between the solvent 1 and the ligand 2 which is defined by the relationship[29]: $\chi_{12} = V_s A_{1,2} / R T + \beta$ with $A_{1,2} = (\delta_{D2} - \delta_{D1})^2 + 0.25(\delta_{P2} - \delta_{P1})^2 + 0.25 (\delta_{H2} - \delta_{H1})^2$ and V_s the volume of the solvent molecule. δ_D, δ_P and δ_H correspond to the Hansen solubility parameters for the dispersion, polar and hydrogen bonding interactions, respectively. β is set equal to 0.34, which corresponds to a value widely used in the literature.[29] This factor is important to obtain a good agreement between experiment and theory as observed elsewhere.[27,28] The magnetic dipole moments are obtained from the saturation magnetization (for cobalt nanocrystals 7.12 10^5 Am^{-1}). The volumes and length of the molecules and the solubility parameters for the ligand and the solvents are taken from reference 29. For the NP surface per ligand 16 $Å^2$ is used, which is a typical value found for NP. The Hamaker constant for the Van der Waals attraction between the cores of the NPs is taken from reference 34. The presence of the solvent medium reduces the Van-der Waals interaction of cobalt compared to the vacuum. This effect is calculated by the usual equations (see reference 34), which leads to a Hamaker constant of 30.0 10^{-20} J for cobalt in hexane, for example.

To estimate the influence of the presence of ethanol in hexane, an average molecular volume and solubility parameter for the solvent mixture are calculated from the following relations: V_s = f(hexane) V_s(hexane) + f(ethanol) V_s(ethanol) and δ_{D1} = f(hexane) δ_{D1}(hexane) + f(ethanol) δ_{D1}(ethanol) (the same equations are applied for δ_{P1} and δ_{H1}). f(hexane) and f(ethanol) is the molar amount of hexane or ethanol in the solvent.

3. Results and discussion

3.1. Control of both the Supercrystallinity and Morphology of Self-Assemblies of Co NCs Comparative Structural Investigation of Supercrystalline Films and Colloidal Crystals

Co NCs, synthesized by chemical reduction in reverse micelles, are coated with dodecanoic acid and characterized by a mean diameter and size polydispersity of 8.1 nm and 11% respectively (Fig. 1a).[31] The electron diffraction pattern (Fig. 1b) shows two diffuse rings at 2.04 and 1.20 ± 0.01 Å, indexed as the (111) and (220) lattice planes of fcc cobalt. The diffuse character of the rings indicates the poor crystallinity of the Co particles, which is further confirmed by the HRTEM pattern (Fig. 1c) revealing the existence of crystallized domains less than 1 nm.[35-37]

3.1.1. Supercrystalline films

By a slow evaporation under a pure nitrogen flow of a colloidal solution of fcc-Co NCs, supercrystals are produced.[32] The scanning electron microscopy (SEM) image in Fig. 1D shows a rather inhomogeneous film, consisting of isolated domains with areas of several ten square micrometers and average thickness of about 1 μm. The corresponding grazing incidence small-angle X-ray scattering (GISAXS) pattern is characteristic of fcc supercrystalline domains sharing a common [111] orientation perpendicular to the surface (Fig. 1e)[32]; an indexation of the various spots is given. The (111) peak width (δ = 0.08 nm^{-1}) is not resolution-limited (0.045 nm^{-1} (Table 1). This indicates that long-range order does not extend over distances higher than 100 nm perpendicular to the substrate. The (111) peak location corresponds to a stacking periodicity ca. 9.0 nm and hence to a centre-to-centre NC distance

($D_{c\text{-}c}$) equal to 11.1 nm; it gives an interparticle distance ($D_{i\text{-}p}$) of 3.0 nm (Table 1) in very good agreement with values previously reported in similar supercrystalline films induced by a heterogeneous layer-by-layer growth.[32,33,37]

In the literature, two different ways to calculate the NC distance in assemblies have been proposed: the OCM (Overlap Cone Model)[24] and the OPM (Optimal Packing Model)[25]. In the following both theories are applied to our experiments. For a reduced ligand length $\lambda = 2l/d_{NC}$ (with l the ligand length (here, 1.77 nm) and d_{NC} the NC diameter), the OCM theory yields the following equation for the reduced interparticle distance $\tau = D_{c\text{-}c}/d_{NC}$:

$$\tau = (\eta(1+3\lambda))^{1/3} \quad (1)$$

η is the volume fraction for cores at contact in the lattice ($\eta = 0.74$ for the FCC lattice).

In the case the OPM theory the following equation for the reduced interparticle distance is obtained:

$$\tau = (1+3\lambda)^{1/3} \quad (1)$$

The OPM theory implies that the tetrahedral voids within the NC superlattice are not occupied with ligand molecules as it has been explained in Reference 24. Recent atomistic simulations[38] have shown that this hypothesis is not correct and that the alkane thiolates fill the whole interstitial space between the NCs in good agreement with the OCM theory. The NC distances obtained by these simulations are in good agreement with the OCM results.

Please note that equations (1) and (2) are strictly valid only for $\lambda > 0.54$, but for the λ of 0.44 obtained here, the equation already gives very reliable results. Applying equations (1) and (2) a value of 1.20 and 1.32 for τ is calculated, in the OCM and OPM respectively. This is smaller than the measured value of 1.37, which shows that the packing of the particles is not optimal. There are several reasons why the value predicted by OCM is difficult to obtain within experiments:

- First, the polydispersity of the particles leads to various distances within the superlattice. In particular, the largest particles limit the approach of the nanocrystals which leads to an increase of the average distance between the particles.
- The packing of the ligands with long alkyl chain may not be optimal due to a rapid formation of superlattices.
- Some residual solvent or not adsorbed ligand molecules may be caught with the interstitial voids.

These reasons explain why often the OPM gives a better agreement with experimental data which does of course not imply the correctness of this theory.

3.1.2. Colloidal crystals with 100 μl of ethanol

We now turn to the sample obtained from the same batch of 8.1 nm Co NCs by ethanol-induced precipitation using an ethanol volume equal to 100 μl (see section 2.4). After total evaporation of the solvent in beaker 1 (containing initially the colloidal solution), that is after roughly 20h, low magnification SEM study shows extensive production of isolated objects (Fig. 1f). A film morphology is not anymore observed and the population is composed of facetted objects in different orientations. This first observation tends to rule out a heterogeneous nucleation process. The facetted objects are characterized by both well-defined morphologies, regular triangles (16%), truncated triangles (13 %) and hexagons (14%), and irregular facetted morphologies (58%). Their size and thickness reach 5 μm and 1μm, respectively. Inserts of Fig. 1f (hexagon and truncated triangle) show that well-developed

facets, clear edges and sharp corners can be observed. After the annealing of the samples at 350°C for 15 min, favoring the decomposition and/or evaporation of the excess of dodecanoic acid, extensive use of the high-resolution SEM technique is allowed. Fig. 2 shows high-magnification SEM images of two morphologies. The high-magnification SEM image (Fig. 2b) associated to a regular hexagonal colloidal crystal (Fig. 2a) exhibits regular stacking of NCs on the top facet with six-fold symmetry (i.e. [111] axis perpendicular to the substrate); terraces and steps are clearly visible. A triangular colloidal crystal exhibits similar crystallographic feature (Fig. 2c-d). Whatever the morphology of the colloidal crystals is, SEM study evidences long-range NC ordering of the top and side facets. Similar to the crystalline films, GISAXS study reveals an fcc superstructure (Fig. 1g). As reported in Table 1, the (111) peak is now resolution-limited in width that indicates higher correlation distances in ordered domains compared to the supercrystalline film. The stacking periodicity in the [111] direction is equal to 8.7 nm that in turn gives $D_{c\text{-}c}$ and $D_{i\text{-}p}$ values equal to 10.6 nm and 2.5 nm respectively. This leads to a reduced interparticle distance τ of 1.30 compared to the values of 1.23 (OCM) and 1.36 (OPM) obtained by the theory. This shows that the packing is close to the optimal limit as predicted by the OCM theory. The smaller distance between the NCs may be due to a reduced polydispersity within the colloidal crystals compared to the films. This implies a more efficient size segregation in case of homogeneous nucleation compared to the heterogenous nucleation.[21,39] This result is in good agreement with reports of a previous study using epsilon-Co NCs coated with oleic acid and dispersed in toluene.[4] The reduced interparticle distance can be translated in the ratio of the volume fraction Φ in NP compared to the maximum value Φm corresponding to NP at contact in the same structure. Here we get $\Phi/\Phi m$= 0,45 and 0,38 for the colloidal crystal and the supercrystalline film respectively.

3.1.3. Colloidal crystals with 800 μl of ethanol

The same deposition performed with increasing the ethanol volume from 100 μl to 800 μl, all other things being equal, also allows the formation of colloidal crystals, which morphologies are almost similar to those obtained with 100 μl of ethanol. (Fig. 3). We observe regular triangles (15%), truncated triangles (15 %) and hexagons (14%), with irregular facetted morphologies (56%). However, we observe that crystals obtained with 800 ul of ethanol (other than regular triangles, truncated triangles and hexagons) are characterized by slightly less regular shapes compared to the crystals obtained with 100 ul of ethanol. In a very reproducible way, we noticed that their mean size (2 μm) is lower compared to the one obtained with 100 μl of ethanol (5 μm). Indeed, the comparative study of the crystal colloidal size obtained with 100 μl and 800 μl of ethanol, repeated 5 times, shows invariably, this size effect. This size effect is in very good agreement with the results obtained for colloidal crystals of maghemite NCs (unpublished data). To better understand the evaporation process, we recorded, as a function of time (t), the evolution of the relative height on both the beaker 1 containing the colloidal solution of NCs in hexane and the beaker 2 containing ethanol, which volume is either 100 μl or 800 μl (see Fig. 4). The relative height of solutions is defined as $[(h(t)/h(t=0)) \times V_0] - V_0$, where h(t) is the height of the solution at time t and V_o, the initial volume on the beakers. For both ethanol volumes, we observe that while the relative height of the colloidal solution of NCs in the hexane beaker continuously decreases due to the evaporation of hexane, it increases in the ethanol beaker due to an absorption of hexane. As shown in Fig. 4, at the early stage of the process (before 100 min), the

evaporation rate of the colloidal solution is the same whatever the ethanol volume is. However, after 100 min, we observe that the evaporation of the colloidal solution is more rapid with 800 μl of ethanol volume compared to 100 μl. Therefore, the total evaporation of the colloidal solution lasts around 8 h in presence of 800 μl of ethanol (initial volume) while it takes around 20 h in presence of 100 μl of ethanol. The more rapid evaporation of the colloidal solution leaves less time for the colloidal crystals to grow within the solution, which leads to their smaller size and slightly less regular shape experimentally observed.

The comparative structural investigation of the supercrystalline film samples and the colloidal crystals obtained with the same batch of Co NCs, clearly evidences that the supercrystalline structure is in both cases fcc. However, Co NC packing is significantly denser and the coherence length higher in colloidal crystals compared to supercrystalline film. To our knowledge, the control of the nucleation of supercrystals, keeping unchanged the size, the coating agent of the NCs and the starting colloidal solvent has never been evidenced elsewhere**.** Indeed, Courty et al. have controlled the supercrystal growth of Ag NCs by changing the coating agent composition (triphenylphosphine/dodecanethiol),[40] while Goubet et al. acted on the size of Au NCs and/or the colloidal solvent.[25,26]

3.1.4. Theoretical Investigation of the Nucleation of Colloidal Crystals made of 8.1 nm-Co NPs.

When NC solutions are evaporated, usually films made of the particles are obtained as previously observed for the deposition without ethanol (Fig. 1d). However, when the solution is evaporated in the presence of ethanol, the formation of isolated well-faceted supercrystals occurs (Fig. 1f). This is usually explained by the appearance of attractive forces between the NCs. Thus for gold NCs, it has been found that for an attractive peak larger than 3 kT, single crystals nucleate and grow during the solvent evaporation.[27,28] Here the interaction between the NCs are computed using the model explained in section 2.6.

The interaction between the cobalt NCs is shown in Fig. 5 for pure hexane and ethanol-hexane mixtures. As the amount of ethanol in hexane increases, the interaction becomes attractive and its amplitude reaches 3 kT for which the formation of isolated supercrystals is expected. According to these calculations, this should happen at an amount of >14 % of ethanol in hexane. The attraction between the particles is due to the term of the free energy of mixing and the high solubility parameters of ethanol compared to those of the ligands. This expresses a stronger attraction between ethanol molecules in contrast to the ligand. The other interaction terms such as the Van-der-Waals interaction of the NC cores or the magnetic dipole-dipole interactions play a minor role.

To verify if the concentration of 15 % necessary for a homogeneous nucleation is reached during the evaporation, the concentration of ethanol in the first beaker with the NCs were measured by gas chromatography with flame ionization detector. The following amounts of ethanol in hexane during the evaporation in presence of ethanol (800 μl): 5, 9, 16 and 13 % after 160, 200, 250 and 310 min, respectively.[22] This shows that the amount of ethanol reached during the evaporation is sufficiently large so that the formation of isolated supercrystals can be explained by the theory.[22] In future, it would be interesting to check these amounts for an ethanol volume of 100 μl.

This leads to the following explanation for the formation of single supercrystals: during the evaporation, the ethanol amount increases in the beaker 1 with the NC solution. At a percentage of

ethanol >14% the formation of single supercrystals occurs due to the attraction between the ligands coating NCs induced by the presence of ethanol.

3.2. Comparative Magnetic Investigation of Supercrystalline Film and Colloidal Crystals of 8.1 nm- Co NCs

Fig. 6a shows the field cooled (FC) and zero field cooled (ZFC) magnetization versus temperature curves measured with an applied field of 2 mT, for both supercrystalline film sample and colloidal crystals composed of dodecanoic acid-coated Co NCs. The ZFC curves present a broad peak at c.a. 104 K for the supercrystalline films and 128K for the colloidal crystals, while the corresponding FC curves present a nearly flat plateau below the ZFC peak temperatures. This latter feature is a well-known characteristic of the collective behavior induced by strong dipole-dipole interactions (DDI). In order to assign the ZFC peak temperature to the physical properties of the supercrystalline systems, we also measured the ZFC curve on the diluted system. This latter measurement was performed with another batch of Co NCs, (batch 2), characterized by a mean diameter of 8.5 nm, slightly larger than those used for the supercrystalline films (8.1 nm). This slight change in diameter is due to the fluctuations obtained from one synthesis to another. To allow accurate study of the interaction effect, supercrystalline films made with the same batch 2 of 8.5 nm Co NCs were also prepared. The temperature T_p of the ZFC peak for the diluted systems and the supercrystalline films are found equal to 84 K and 120 K respectively. The important point here is that the ZFC peak of the diluted system, which is unambiguously assigned to the isolated NC blocking temperature, is much smaller than the ZFC peak of the supercrystalline structures ones. Correcting for the slight difference in size, we can infer that the blocking temperature of NCs of the first batch is c.a. 72 K. This is in agreement with previous results[41] for isolated fcc cobalt NP of 7 nm. Hence, such a difference shows that the ZFC peak of the supercrystalline films and the colloidal crystals is not a blocking temperature due to individual particle anisotropy but instead can be assigned to the freezing temperature resulting from the DDI induced collective behavior. From the value of T_b, we can deduce an effective uniaxial anisotropy constant of c.a. 1.01 $10^5 Jm^{-3}$. We have not measured the saturation magnetization M_s of our Co NCs but nevertheless, we can deduce an estimated value from the known results for polycrystalline Co NPs synthesized following a similar route[42], namely $M_s \sim 80$ emu/g (7.12 10^5 A/m). This leads to an anisotropy to DDI coupling ratio, given by $(24/\mu_0)(K/M_s^2)(\Phi_m/\Phi)$ where Φ and Φ_m are the NP volume fraction and its maximum value in the FCC lattice (0.74), larger that 8.5 with the values of (Φ_m/Φ) determined above. We can then conclude by assuming a random distribution of NC easy axes that the supercrystalline structures are in the super spin glass (SSG) region of the magnetic phase diagram.[10,14] The ZFC peak temperatures are thus assigned to the paramagnetic (PM)/SSG transition slightly smaller than $T_r = (\mu_0/4\pi k_B)(\pi/M_s)^2 d_{NC}^3(\Phi/\Phi_m)$ as deduced from theoretical simulations.[15,16] A precise determination of the freezing temperature Tp is not possible due to the lack of a precise value of Ms ; however the upper bond, Tr, is in between 176K and 214 K for $\Phi/\Phi m = 0.38$ corresponding to the supercrystalline film with Ms in between 70 and 85 emu/g and $d_{NC} = 8.1$ nm and respectively between 203 K and 247 K for $d_{NC} = 8.5$ nm. We can

corroborate our interpretation by noting that the supercrystalline film to the colloidal crystals Tp ratio follows the corresponding volume fractions ratio namely 0.81 versus 0.85 respectively where the volume fraction ratio is obtained from the ratio of the t-3 values. Notice that the same method as above was used to assign the ZFC peak temperatures to the freezing one of compact systems made of maghemite NCs. 15

Fig. 6b shows the hysteresis curves for the supercrystalline film sample and the colloidal crystals, performed at 3 K. In both cases, the magnetic behavior is almost similar to that previously observed for the supercrystalline film sample of Co NCs.[7] Whatever the supercrystal morphology is, saturation is reached at around 4 T with the same ratio of remanent-to-saturation magnetization (M_r/M_s) of 0.5. However, the coercive field (H_c) is higher for the colloidal crystals (92 mT) compared to the supercrystalline film (85 mT) (Table 1).

This behavior is attributed to the higher shape anisotropy in the colloidal crystals compared to the supercrystalline film, arising from the increased coherence length assembly (Table 1). This behavior is coherent with the difference in magnetic behavior at high field, observed in poorly anisotropic disordered assemblies and highly anisotropic supercrystalline films, both composed of Co NCs.[42]

Thanks to the use of the same batch of Co NCs to form the two supercrystalline morphologies, an accurate comparative magnetic study can be performed and evidences, for the first time, the increase in both magnetic dipolar interactions and in coherence length in the fcc colloidal crystals compared to the fcc supercrystalline films.

4. Conclusions

By using the same batch of dodecanoic acid-coated Co NCs, synthesized by the micellar approach, i.e., characterized by the same size polydispersity, the same coating agent and dispersed in the same solvent, this study evidences that the unique control of the solvent mediated ligand-ligand interaction gives rise to either supercrystalline film or colloidal crystals of Co NCs. Colloidal crystals are characterized by (truncated) triangular and hexagonal morphologies. Similar to the supercrystalline films, and thanks to GISAXS technique, their supercrystallinity is identified without any ambiguity as fcc, with, however, a much higher density packing and coherence length. The change of the supercrystalline morphology is explained by a modification of the nucleation mechanism. Colloidal crystals formation results from the appearance of attraction between the NCs due to the presence of ethanol in the solvent. Theoretical calculations allow predict the onset of the new type of supercrystal growth in good agreement with the experiment. A decrease of the particle distance is observed for the colloidal crystals compared to supercrystalline film. The results are closer to the limit of ideal packing of ligands predicted by the OCM theory. The enhanced structural and magnetic properties (coherence length and magnetic dipolar interaction) of the colloidal crystals compared to the supercrystalline film composed with the same Co NCs, are evidenced.

Acknowledgements

FEG-SEM instrumentation was done at the Institut des Matériaux de Paris Centre (IMPC FR2482) and was funded by Sorbonne Université, CNRS and by the C'Nano projects of the Région Ile-de-France.

Fig. Captions

Fig. 1 (a) TEM image of 2D assembly of 8.1 nm cobalt nanoparticles, (b) corresponding electron diffraction pattern and (c) HRTEM image of a single nanoparticle. SEM images of (d) supercrystalline film and (e) corresponding GISAXS pattern. (f) Colloidal crystals (100 μl of ethanol). Insets: high-magnification SEM images of truncated triangular and hexagonal platelets and (g) corresponding GISAXS patterns.

Fig. 2 SEM-FEG images observed at different magnifications of colloidal crystals (100 μl of ethanol). (a, b) regular hexagons on top view, (c, d) regular hexagons or truncated triangle on side view.

Fig. 3 SEM images of colloidal crystals (a) 800 μl, (b) 100 μl of ethanol.

Fig. 4 Selected photographs of the two beakers containing solutions of Co nanocrystals in hexane (B1) and ethanol (B2) at initial state (a) and after 300 min (b) during the evaporation process.
Evolution of the relative height of solutions on the beakers for initial volume, V_0, solutions of nanocrystals in 200 μl of hexane (**X**, +) and with either 800 μl (Δ) or 100 μl (**O**) of ethanol as a function of time.

Fig. 5 Interaction energy between two dodecanoic acid coated 8.1 nm cobalt nanocrystals as a function of the particle distance for different amounts of ethanol in hexane.

Fig. 6 (a) Temperature dependence of the magnetization in the zero-field cooled/field cooled (ZFC/FC) curves with applied field H = 2 mT and (b) hysteresis curves performed at 3K of colloidal crystals (dashed line) and supercrystalline film (solid line) composed of 8.1 nm fcc-Co NPs.

Table 1: Structural parameters extracted from GISAXS analysis for the different supercrystalline samples: d_{111} ((111) stacking periodicity), δ (width at half maximum of 111 Brag's peak), D_{cc} (center-to-center particle distance) and D_{ip} (interparticle distance considering the nanoparticle size equal to 8.1 nm).

Fig. 1

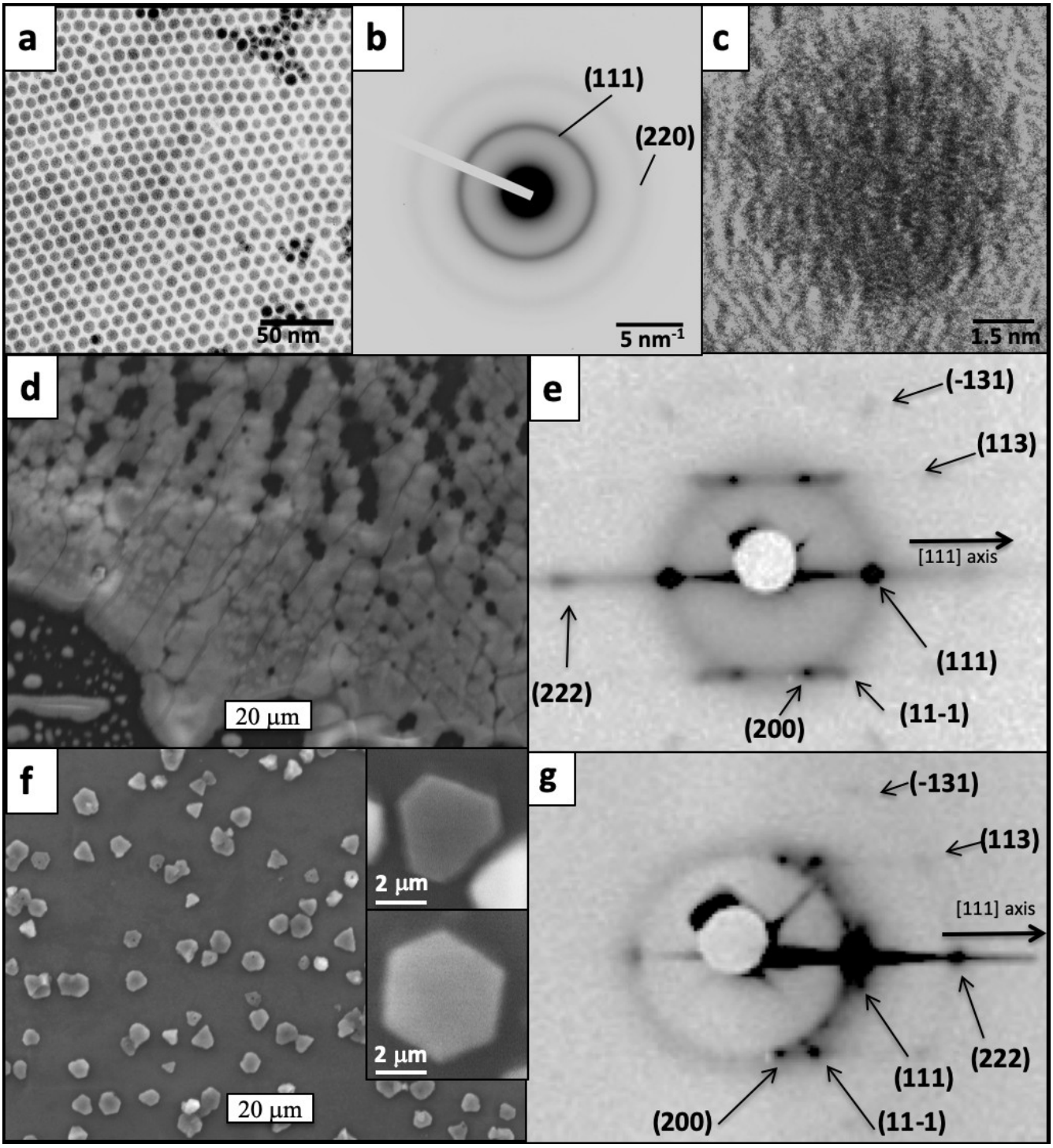
a
50 nm
b
(111)
(220)
5 nm-1
c
1.5 nm
d
20 μm
e
(-131)
(113)
[111] axis
(111)
(222)
(200)
(11-1)
f
2 μm
2 μm
20 μm
g
(-131)
(113)
[111] axis
(222)
(111)
(200)
(11-1)

Fig.2

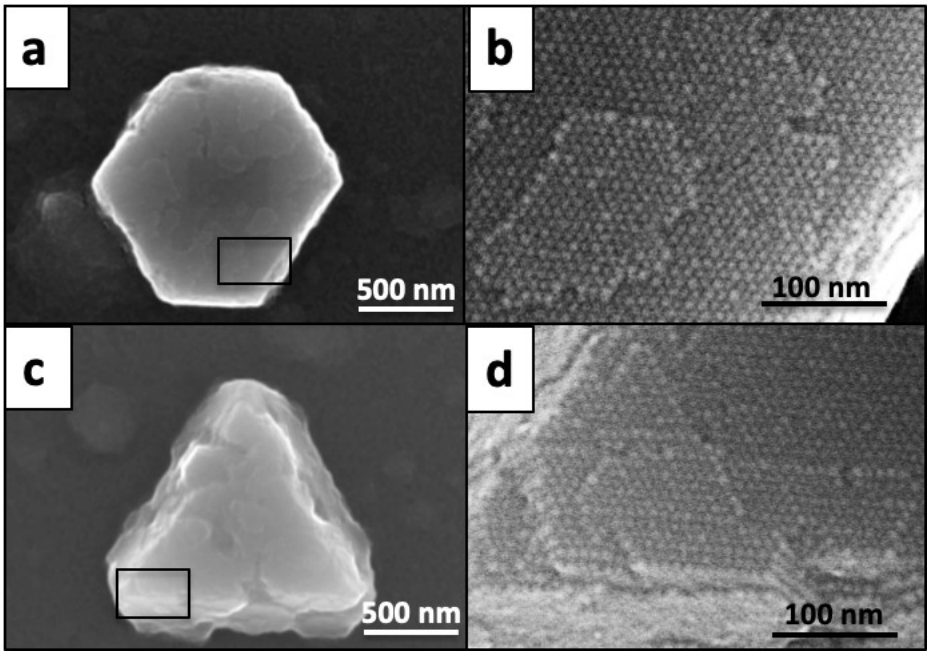

Fig. 3

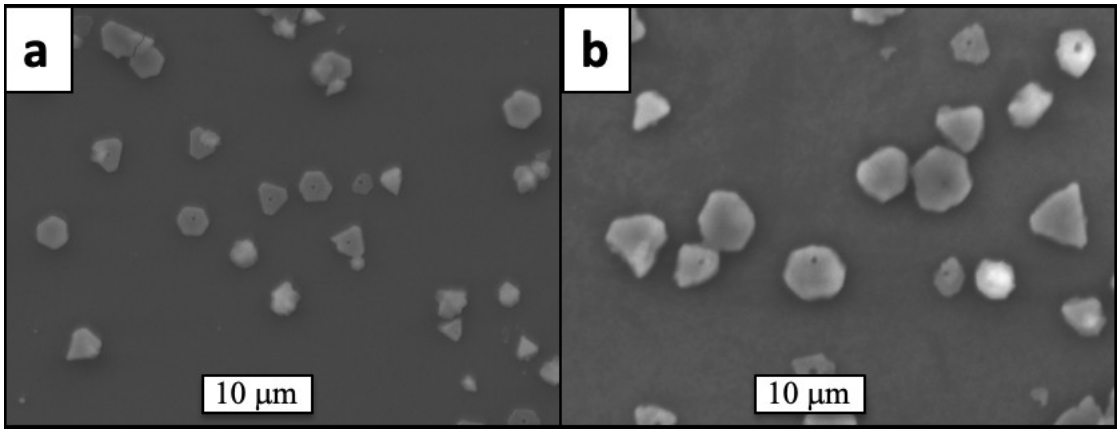

Fig. 4

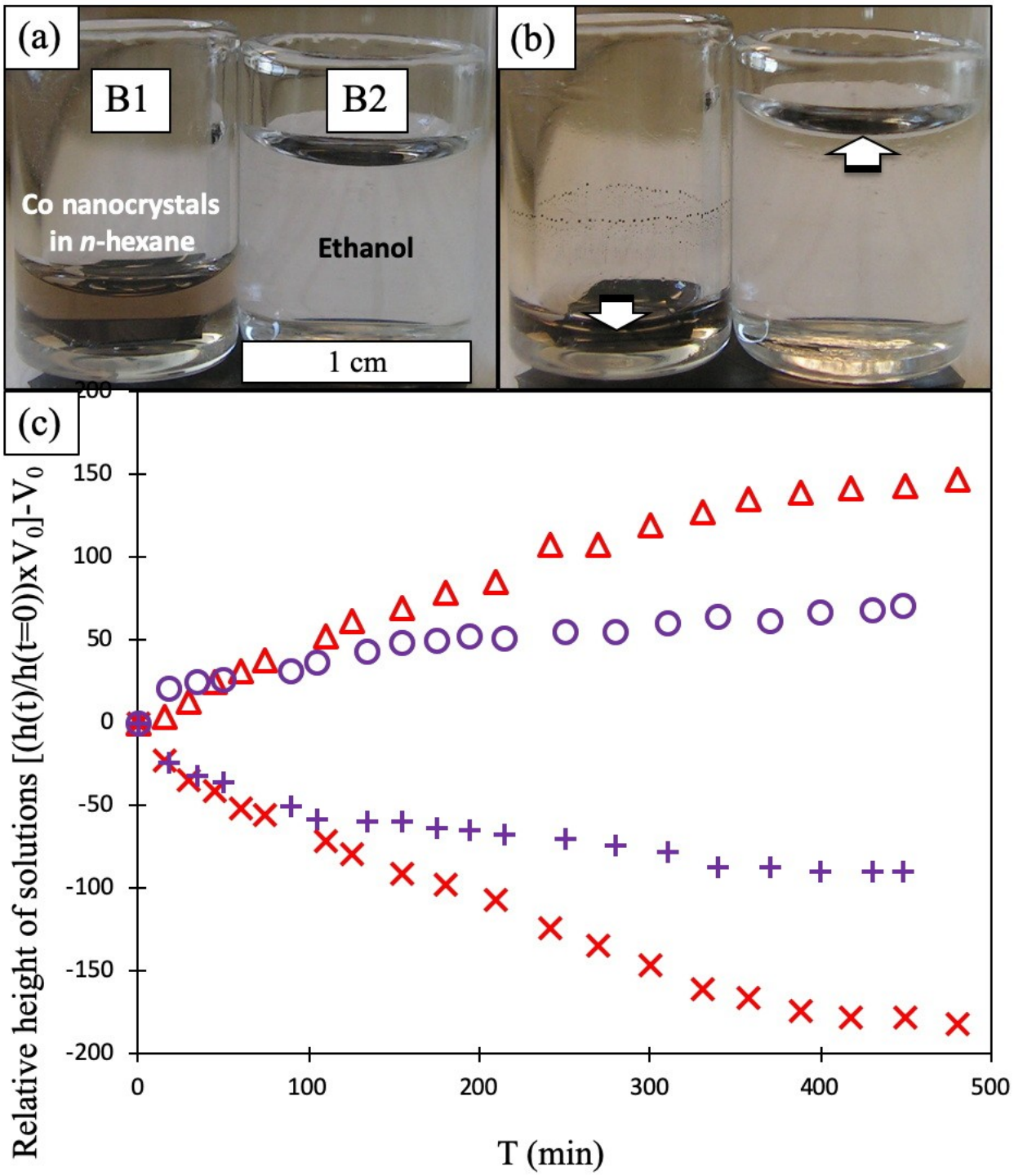
(a)
B1
B2
Co nanocrystals
in n-hexane
Ethanol
1 cm
(b)
(c)
Relative height of solutions [(h(t)/h(t=0))xV0]-V0
T (min)
200
150
100
50
0
-50
-100
-150
-200
0
100
200
300
400
500

Fig. 5

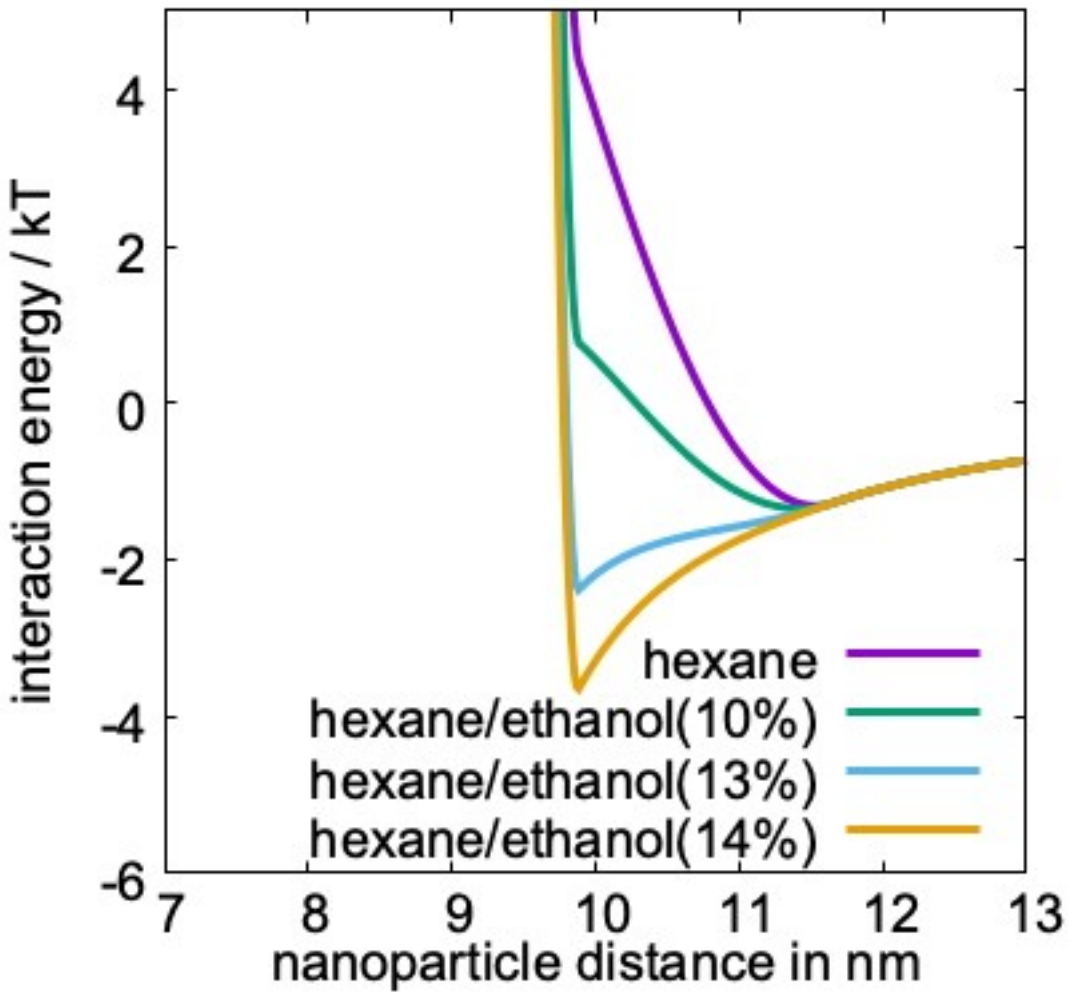
interaction energy / kT
4
2
0
-2
-4
-6
7
8
9
10
11
12
13
nanoparticle distance in nm
hexane
hexane/ethanol(10%)
hexane/ethanol(13%)
hexane/ethanol(14%)

Fig. 6

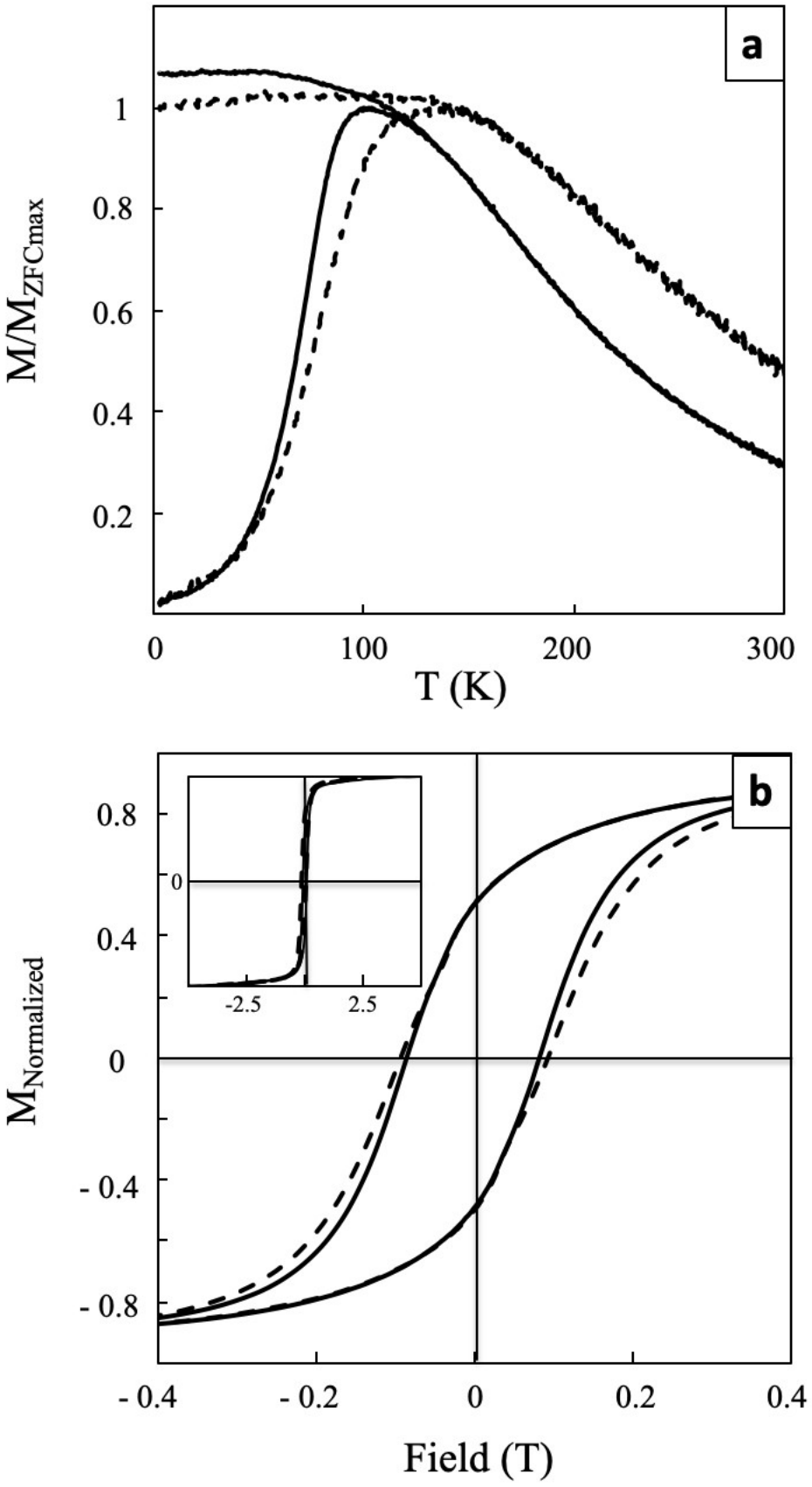
a
1
0.8
0.6
0.4
0.2
M/M_ZFCmax
0
100
200
300
T (K)
b
0.8
0.4
0
- 0.4
- 0.8
M_Normalized
0
-2.5
2.5
- 0.4
- 0.2
0
0.2
0.4
Field (T)

Table 1

Structural parameters	Supercrystalline films	Colloidal crystals
d_{111} ±0.1nm	9.0	8.7
δ ± 0.01 nm	0.08	0.05
D_{cc} ±0.1 nm	11.1	10.6
D_{ip} ±0.1 nm	3.0	2.5
T_B (K)	104	128
M_r/M_s	0.5	0.5
H_c (mT)	85	92

Notes and references

1 I. Lisiecki, *Acta Phys. Pol. A*, 2012, **121**, 426–433.

2 A. M. Kalsin, M. Fialkowski, M. Paszewski, S. K. Smoukov, K. J. M. Bishop and B. A. Grzybowski, *Science*, 2006, **312**, 420–424.

3 M. A. Boles, M. Engel and D. V. Talapin, *Chem. Rev.* 2016, **116**, 11220–11289.

4 M. Gauvin, N. Yang, E. Barthel, I. Arfaoui, J. Yang, P. A. Albouy and M. P. Pileni, *J. Phys. Chem. C*, 2015, **119**, 7483–7490.

5 J. J. Urban, D. V Talapin, E. V. Shevchenko, C. R. Kagan and C. B. Murray, *Nat. Mater.* 2007, **6**, 115–121.

6 A. Courty, I. Lisiecki and M. P. Pileni, *J. Chem. Phys*, 2002, **116**, 8074–8078.

7 D. Parker, I. Lisiecki, C. Salzemann and M. P. Pileni, *J. Phys. Chem. C*, 2007, **111**, 12632–12638.

8 S. Mørup, *Hyperfine Interact,* 1994, **90**, 171–185.

9 P. E. Jönsson, *Adv. Chem. Phys.* 2004, **128**, 191–248.

10 D. Parker, I. Lisiecki, and M. P. Pileni. *J. Phys. Chem. Lett*, 2010, **1**, 1139–1142.

11 S. Hariharan, J. Gass, *Rev. Adv. Mater. Sci*, 2005, **10**, 398–402.

12 H. Zeng, J. Zhang, C. Kuang and M. Yue, *Appl. Nanosci*, 2011, **1**, 51–57.

13 S. Bedenta, T. Eimüller, W. Kleemann J. Rhensius, F. Stromberg, E. Amaladass, S. Cardoso, and P. P. Freitas, *Phys. Rev. Lett*, 2007, **98**, 176601-176604.

14 V. Russier and E. Ngo, *Condensed Matter Physics*, 2017, **20**, 33703-33713.

15 J. J. Alonso, B. Allés and V. Russier, *Phys. Rev. B,* 2019, **100**, 134409.

16 V. Russier and J. J. Alonso, *J. Phys: Condensed Matter*, 2020, **32**, 135804.

17 M. Li, Y. Chen, N. Ji, D. Zeng and D. L. Peng, *Mater. Chem. Phys*, 2014, **147**, 604–610.

18 L. Meng, W. Chen, Y. Tan, L. Zou, C. Chen, H. Zhou, Q. Peng and Y. Li, *Nano Res.* 2011, **4**, 370–375.

19 O. Kasyutich, R. D. Desautels, B. W. Southern and J. Van Lierop, *Phys. Rev. Lett.* 2010, **104**, 1–4.

20 L. Meziane, C. Salzemann, C. Aubert, H. Gérard, C. Petit and M. Petit, *Nanoscale* 2016, **8**, 18640–18645.

21 N. Yang, Z. Yang, M. Held, P. Bonville, P. A. Albouy, R. Lévy and M. P. Pileni, *ACS Nano* 2016, **10**, 2277–2286.

22 A. Ngo, S. Costanzo, P. A. Albouy, V. Russier, S. Nakamae, J. Richardi and I. Lisiecki, *Colloids and Surfaces A* 2019, **560**, 270-277.

23 E. Josten, E. Wetterskog, E. Glavic, P. Boesecke, A. Feoktystov, E. Brauweiler-Reuters, U. Rücker, G. Salazar-Alvarez, T. Brückel and L. Bergström, *Sci. Rep*. 2017, **7**, 2802.

24 U. Landman and W. D. Luedtke, Faraday Discuss. 2004, **125**, 1–22.

25 P. Schapotschnikow and T. J. H. Vlugt, *J. Chem. Phys.* 2009, **131**, 124705.

26 D. V. Talapin, E. V. Shevchenko, A. Kornowski, N. Gaponik, M. Haase, A. L. Rogach and H.

Weller, *Adv. Mater.* 2001, **13**, 1868–1871.
27 N. Goubet, J. Richardi, P. A. Albouy and M. P. Pileni, *J. Phys. Chem. Lett.* 2011, **2**, 417–422.
28 N. Goubet, J. Richardi, P. A. Albouy and M. P. Pileni, *Adv. Funct. Mater.* 2011, **21**, 2693–2704.
29 C. Hansen, *Hansen Solubility Parameters. Boca Raton: CRC Press.*; Boca Raton, C. P., Ed.; 2000.
30 C. Petit, P. Lixon and M. P. Pileni, *Langmuir* 1991, **7**, 2620–2625.
31 I. Lisiecki and M. P. Pileni, *Langmuir* 2003, **19**, 9486–9489.
32 I. Lisiecki, P. A. Albouy and M. P. Pileni, *Adv. Mater.* 2003, **15**, 712–716.
33 I. Lisiecki, P. A. Albouy and M. P. Pileni, *J. Phys. Chem. B* 2004, **108**, 20050–20055.
34 J. Israelachvili, *Intermolecular and Surface Forces 3rd Edition*; Press, A., Ed.; Burlington, 2011.
35 M. Cavalier, M. Walls, I. Lisiecki and M. P. Pileni, *Langmuir* 2011, **27**, 5014–5020.
36 Z. Yang, M. Cavalier, M. Walls, P. Bonville, I. Lisiecki and M. P. Pileni, *J. Phys. Chem. C* 2012, **116**, 15723–15730.
37 I. Lisiecki, C. Salzemann, D. Parker, P. A. Albouy and M. P. Pileni, J. Phys. Chem. C 2007, **111**, 12625-12631.

38 T. Djebaili, Thesis, « Simulations atomistiques des interactions des nanoparticules d'or », 2004.
39 X. Lin, C. Sorensen and K. J. Klabunde, *J. Nanoparticle Res.* 2000, **2**, 157–164.
40 K. Ouhenia-Ouadahi, A. Andrieux-Ledier, J. Richardi, P. A. Albouy, P. Beaunier, P. Sutter, E. Sutter and A. Courty, *Chem. Mater.* 2016, **28**, 4380–4389.
41 C. Petit, Z. L. Wang and M. P. Pileni, *J. Phys. Chem. B 2005,* **109***, 15309-15316.*
42 I. Lisiecki, D. Parker, C. Salzemann and M. P. Pileni, *Chem. Mater.* 2007, **19**, 4030–4036.